PHILOSOPHICAL TRANSACTIONS A

royalsocietypublishing.org/journal/rsta

Research

Cite this article: Moore L, Moses JI, Melin H, Stallard TS, O'Donoghue J. 2020 Atmospheric implications of the lack of H_3^+ detection at Neptune. *Phil. Trans. R. Soc. A* **378**: 20200100. http://dx.doi.org/10.1098/rsta.2020.0100

Accepted: 2 July 2020

One contribution of 18 to a discussion meeting issue 'Future exploration of ice giant systems'.

Subject Areas:
solar system, observational astronomy

Keywords:
aeronomy, ionosphere, H_3^+

Author for correspondence:
L. Moore
e-mail: moore@bu.edu

Atmospheric implications of the lack of H_3^+ detection at Neptune

L. Moore[1], J. I. Moses[2], H. Melin[3], T. S. Stallard[3] and J. O'Donoghue[4]

[1]Boston University, Boston, MA, USA
[2]Space Science Institute, Boulder, CO, USA
[3]University of Leicester, Leicester, UK
[4]JAXA Institute of Space and Astronautical Science, Tokyo, Japan

LM, 0000-0003-4481-9862; JM, 0000-0002-8837-0035; HM, 0000-0001-5971-2633; TSS, 0000-0003-3990-670X; JOD, 0000-0002-4218-1191

H_3^+ has been detected at all of the solar system giant planets aside from Neptune. Current observational upper limits imply that there is far less H_3^+ emission at Neptune than rudimentary modelling would suggest. Here, we explore via modelling a range of atmospheric conditions in order to find some that could be consistent with observational constraints. In particular, we consider that the upper atmosphere might be much cooler than it was during the 1989 Voyager 2 encounter, and we examine the impact of an enhanced influx of external material that could act to reduce H_3^+ density. Resulting ionosphere models that are consistent with existing H_3^+ observational constraints have an exospheric temperature of 450 K or less, 300 K lower than the Voyager 2 value. Alternatively, if a topside CO influx of 2×10^8 cm^{-2} s^{-1} is imposed, the upper atmospheric temperature can be higher, up to 550 K. The potential cooling of Neptune's atmosphere is relevant for poorly understood giant planet thermospheric energetics, and would also impact aerobreaking manoeuvers for any future spacecraft. Such a large CO influx, if present, could imply Triton is a very active moon with prominent atmospheric escape, and/or that Neptune's rings significantly modify its upper atmosphere, and the introduction of so much exogenic material would complicate interpretation of the origin of species observed in Neptune's lower atmosphere.

This article is part a discussion meeting issue 'Future exploration of ice giant systems'.

THE ROYAL SOCIETY PUBLISHING

1. Introduction

The H_3^+ ion is rapidly formed primarily by collisions between H_2 and H_2^+ and is therefore expected to be important in a variety of astronomical environments [1,2]. Since its first remote detection in Jupiter's auroral ionosphere [3], it has served as a remarkably useful probe of upper-atmospheric densities, temperatures and velocities at Jupiter (e.g. [4–6]), Saturn (e.g. [7,8]) and Uranus [9], but it has remained undetected thus far at Neptune [10]. Such remote measurements serve as effective constraints in an otherwise difficult-to-sample atmospheric region. They also provide key insights into coupling processes from above and below, as the simplicity of the chemistry in gas giant ionospheres, which consist mainly of H_3^+ and H^+ above the homopause, is temporarily disrupted by any exogenic material [11].

Observations of quantities relevant to H_3^+ in Neptune's upper atmosphere are limited by its distance and small angular size. Voyager 2, during its 1989 flyby, used solar occultation measurements to derive an exospheric temperature of 750 ± 150 K [12], and found stratospheric temperatures of approximately 170 K [13,14]. Interpolated temperature at the expected H_3^+ altitudes is roughly 550 K. Recent ground-based observations have used this average temperature to place an upper limit on H_3^+ column density, based on a non-detection of bright H_3^+ lines near 4 μm, of $1.0^{+1.2}_{-0.16} \times 10^{13}\,\mathrm{m}^{-2}$ [10] (see also [15,16]). These vibration–rotation transitions of the ν_2 fundamental band [17] have been used to derive non-auroral H_3^+ column densities at Jupiter, Saturn and Uranus, typically of order $10^{15}\,\mathrm{m}^{-2}$ [18], $10^{16}\,\mathrm{m}^{-2}$ [8] and $10^{15}\,\mathrm{m}^{-2}$ [9], respectively.

Consistent with the limited observational constraints, there are few published models of Neptune's upper atmosphere. Lyons [19] modelled the sharp layers of electron density revealed by radio occultation experiments in Neptune's lower ionosphere [20]. While that model truncates at 1500 km altitude (above the 1 bar pressure level), the modelled H_3^+ column density can be conservatively estimated as $> 5 \times 10^{13}\,\mathrm{m}^{-2}$, i.e. more than a factor of 5 larger than the current upper limit. A recent model, again focused on Neptune's lower ionosphere, finds an H_3^+ column density that is roughly comparable or even larger [21]. Therefore, while modelling studies of Neptune's ionosphere are limited, with objectives other than upper atmospheric H_3^+, there appears to be a significant discrepancy between the amount of H_3^+ expected and historical observational upper limits.

Here, we conduct a range of model simulations in order to find combinations of conditions in Neptune's upper atmosphere that could be consistent with the present lack of H_3^+ detection. As H_3^+ emission is driven exponentially by temperature, we first examine the possibility that Neptune's atmosphere is cooler than found by Voyager 2 in 1989. Next, as H_3^+ reacts readily with other molecules, we also investigate how its density might be reduced by enhanced influxes of external material, such as CO or dust particles from Triton/other satellites/Neptune's rings, or material from elsewhere in the local system. The models used and modelling approaches followed are described in §2. Results are introduced and discussed in §3, with implications for Neptune's atmosphere outlined in §4.

2. Methods

(a) Model description

The majority of H_3^+ ions in giant planet ionospheres are in photochemical equilibrium (PCE), as the H_3^+ chemical lifetime is much shorter than the transport timescale at most altitudes, and therefore the ion continuity equation simplifies to equating local production and loss (i.e. $P_s = L_s$) [22,23]. While transport processes are still relevant—and highly so for H^+, especially at high altitude—the dominance of chemical loss at low altitudes justifies the use of one-dimensional (1-D) simulations for those regions, which offer the advantages of simplicity and computational freedom over more dynamically comprehensive 3-D simulations.

Two models are adopted in the present work. The simulations are conducted in 1-D, owing to the prevalence of PCE for H_3^+ distributions, and there are separate neutral and plasma modules in order to enable a more computationally efficient exploration of ion chemistry.

The neutral module is described in detail by Moses & Poppe [24], and is actually a combination of a meteoroid ablation code [25,26] with the Caltech/JPL 1-D KINETICS photochemical model [27,28]. KINETICS solves the coupled mass-continuity equations as a function of pressure, and includes molecular and eddy diffusion transport terms. It has proved to be effective and highly adaptable, having been applied to all of the giant planets, and currently treats 70 hydrocarbon and oxygen species that interact via approximately 500 recently-updated chemical reactions [24,29]. Input for the meteoroid ablation code follows from revised constraints on interplanetary dust fluxes in the outer Solar System based on *in situ* spacecraft data [30]. The resulting oxygenated and hydrocarbon mixing ratios are in agreement with a wide range of observational constraints [24]. Therefore, after adjusting the KINETICS simulations for the solar and geometric conditions explored here, the resulting neutral atmospheres serve as an excellent background for exploring realistic ion-neutral photochemistry at Neptune.

Plasma densities and temperatures follow from another 1-D model called BU1DIM, which has recently been generalized for application to any planetary atmosphere, and includes significantly expanded chemistry (see [31] and references therein). BU1DIM describes the time- and altitude-dependent structure of an ionosphere by solving the coupled continuity, momentum and energy equations for all ion species of interest. The primary effect of magnetic fields on 1-D ionospheric calculations is to constrain the plasma motion (e.g. introducing a $\sin^2 I$ term into the expression for vertical ion drift velocity, where I is the magnetic dip angle [32,33]). Therefore—partly due to incomplete knowledge of Neptune's magnetic field, and partly due to the predominance of PCE at H_3^+ altitudes—magnetic field lines are considered to be vertical here. Modelled ion production rates follow from the attenuation of solar Extreme UltraViolet (EUV; 10–124 nm) and soft X-ray photons (combined, the XUV) [34], which are extrapolated to Neptune based on measurements from the Thermosphere Ionosphere Mesosphere Energetics and Dynamics Solar EUV Experiment (TIMED/SEE) [35]. Aside from solar XUV radiation, no other sources of ionization are considered in this work.

Early theoretical models of giant planet ionospheres predicted electron densities that were up to an order of magnitude too large based on later spacecraft measurements, with Saturn exhibiting the most extreme discrepancy [36,37]. One commonly adopted mechanism for reducing modelled electron densities in order to better match observations was to convert H^+ into a short-lived molecular ion via the reaction

$$H^+ + H_2(v \geq 4) \rightarrow H_2^+ + H. \tag{2.1}$$

Without the introduction of some form of ion-neutral charge-exchange reaction, such as (2.1), modelled H^+—and hence electron density, n_e—is unrealistically large, as the radiative recombination rate coefficient for H^+ is extremely slow (approximately 10^{-12} cm^3 s^{-1} for typical giant planet thermospheric electron temperatures) [38]. The (2.1) reaction rate is thought to be near its maximum kinetic value [39,40], however the fraction of molecular hydrogen in the fourth or higher vibrational state is not constrained by observations at present. As two of the dominant sources of vibrationally excited H_2 have been shown to be photon-induced fluorescence and dissociative recombination of H_3^+ ions—two solar-driven processes—we scale fractional H_2 vibrational populations calculated for Jupiter [41] by $1/r^2$ to account for the diminution of solar photons with distance. Thus adjusted, the Majeed *et al.* [41] $H_2(v \geq 4)$ results are then interpolated onto the appropriate Neptune pressure grid. Further model inputs and specific settings are discussed in relation to their corresponding results in §2b.

(b) Variations in the background atmosphere

Planetary H_3^+ emission is optically thin [18] and depends on the temperature and density of the plasma. Therefore, the lack of H_3^+ detection at Neptune is most likely caused by some combination

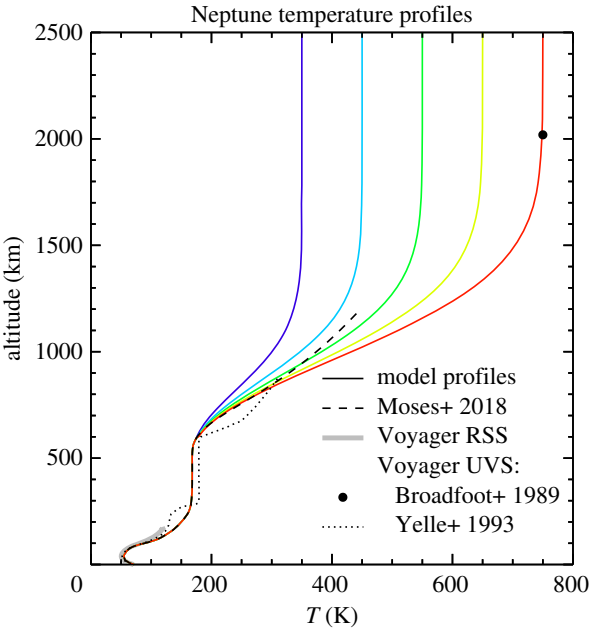

Figure 1. Coloured solid lines represent variations in thermal structure explored in this study. The red is the reference atmosphere based on infrared observations [42], combined in Moses *et al.* [43], and Voyager 2 constraints from its 1989 flyby [12,13], with various aspects of the Voyager data indicated by the grey shaded and dotted lines, and the filled circle. (Online version in colour.)

of two factors: (a) Neptune's upper atmosphere is cooler than found by Voyager 2 in 1989, and/or (b) there is some unknown mechanism reducing the amount of H_3^+ in Neptune's ionosphere. This section outlines the parameter variations that we explore in order to find model atmospheres that are consistent with the present H_3^+ upper limit.

Constraints on thermal structure in Neptune's atmosphere are based on analysis of Voyager 2 flyby data and on a variety of infrared observations. Solar occultation measurements by Voyager's Ultraviolet Spectrometer (UVS) found the topside, or exospheric (T_{exo}), temperature to be 750 ± 150 K [12] (filled circle in figure 1). Radio occultations by Voyager's Radio Science Subsystem (RSS), sensitive to the upper troposphere and lower stratosphere, found a local minimum of approximately 50 K [20] (grey shaded region in figure 1). Subsequent detailed analysis of the UVS observations was also used to constrain temperatures in the upper stratosphere [13] (dotted line in figure 1). Finally, remote infrared observations [42,44] led to a temperature profile in Neptune's troposphere and stratosphere that was mostly consistent with Voyager data (approximately represented by the dashed line in figure 1, taken from [43]).

The thermal structure used in the reference model is given by the red curve in figure 1. Other coloured curves represent additional possible atmospheres that are still consistent with observations in the troposphere and stratosphere, differing only in exospheric temperature and the resulting upper atmospheric temperature gradient. There is sufficient justification for considering exospheric temperatures different from what Voyager observed in 1989. First, the Voyager measurement sampled one location on Neptune, so it is reasonable to assume that temperature will vary spatially. Second, we know that temperatures in giant planet upper atmospheres—and, of course, planetary atmospheres in general—are temporally variable. There is recent evidence at Saturn [45,46] and Uranus [9] for significant temperature variations as well as long-term cooling. Finally, we do not yet fully understand the energetics of giant planet upper atmospheres: observed exospheric temperatures at all four giant planets are hundreds of Kelvin hotter than predictions based on solar heating alone [47]. Upper atmospheric energy budgets are

likely further modified by internal forcing, such as due to gravity waves, which have been shown to be present at Jupiter [48] and Saturn [49], though the degree of resulting heat deposition is unclear at present [50].

Thermal structure primarily affects overall atmospheric extent. It also strongly affects H_3^+ emission, as it is driven exponentially by temperature [51]. Also relevant for the lack of H_3^+ detection at Neptune is H_3^+ column density, which is marginally reduced in a cooler atmosphere, owing to a smaller column depth. H_3^+ is also highly reactive, however, and so can be removed by contaminants introduced into the pristine H^+ and H_3^+ upper ionosphere. At Saturn, we now have ample evidence for an inflow of ring material modifying ionospheric chemistry [8,11,52,53]. All of the giant planets are also exposed to interplanetary dust particles (IDPs), primarily from various families of comets. Dust grains can also originate from active plumes on satellites such as Io, Enceladus and Triton. Constraints on these influxes are limited, typically based on model comparisons with observations sensitive to atmospheric constituents at stratospheric pressure levels. In other words, such model-data comparisons are insensitive to possible upper-atmospheric concentrations, and those concentrations are responsible for modifying H_3^+ densities. Further ionospheric modifications might derive from internal forcing, such as due to gravity waves breaking in the lower thermosphere, though the effect on H_3^+ is minimal due to its relatively short chemical lifetime [54].

The upper-atmospheric 'contaminant' explored here is CO. While the reference atmosphere contains both internal and external sources of CO [43], only external sources lead to sufficient thermospheric abundances to affect the ionosphere. It acts to remove H_3^+ via charge-exchange reactions, just as a range of other possible contaminants would. Given the lack of upper-atmospheric observational constraints, we choose to focus on CO for simplicity, but emphasize that some combination of contaminants could similarly affect the ionosphere. In addition, there is an enormous CO abundance in Neptune's stratosphere, which must have an external source based on the increase of the observed mixing ratio from the troposphere to stratosphere (e.g. [55]). Current literature tends to favour a cometary impact within the last couple of hundred years as that source (e.g. [21,24] and references therein), however models which consider a topside influx of $\leq 2 \times 10^8$ CO molecules $\mathrm{cm^{-2}\,s^{-1}}$ are also consistent with stratospheric constraints on CO and lead to much larger thermospheric CO concentrations than the cometary scenario [24].

Figure 2*a* presents the reference Neptune atmosphere used in this study, representative of conditions at 45° S planetocentric latitude. Its vertical structure follows from the red temperature profile in figure 1, and its oxygenated species are generated by two sources: a flux of IDPs based on recent dust dynamical modelling [30], and a large cometary impact approximately 200 years ago (as described in [24]). Figure 2*b* then illustrates the full range of variations in CO evaluated. First, solid lines correspond to the above scenario, coloured according to the assumed T_{exo}. Second, dotted lines consider that Neptune's CO is due solely to IDPs, also coloured by T_{exo}. Note that solid and dotted lines only differ below 600 km altitude (i.e. they overlap above 600 km), demonstrating that higher altitude CO comes from IDPs in the reference model. Finally, a range of different topside influxes of CO are represented by various types of dashed lines, as indicated in the legend. The five different thermal scenarios illustrated in figure 1 are all evaluated for the maximum CO influx of 2×10^8 $\mathrm{cm^{-2}\,s^{-1}}$, colour coded according to T_{exo}. For reduced CO influxes, spanning 10^5–10^8 $\mathrm{cm^{-2}\,s^{-1}}$ only the $T_{exo} = 750$ K atmosphere is considered.

Finally, it should be noted that modifying the effective rate of reaction (2.1) is likely not a primary solution to the lack of H_3^+ at Neptune. A larger electron density, such as would follow from a reduced (2.1) rate, would lead to smaller H_3^+ densities via an increase in their dissociative recombination reaction with electrons, but electron densities are constrained to be $< 10^3$ $\mathrm{cm^{-3}}$ above approximately 1700 km altitude by Voyager 2 radio occultation measurements [20].

3. Results and discussion

We now present ionospheric results based on the neutral atmospheres shown in figure 2. In 3a, we show altitude variations in H_3^+ number density. In 3b, we column-integrate the model parameters

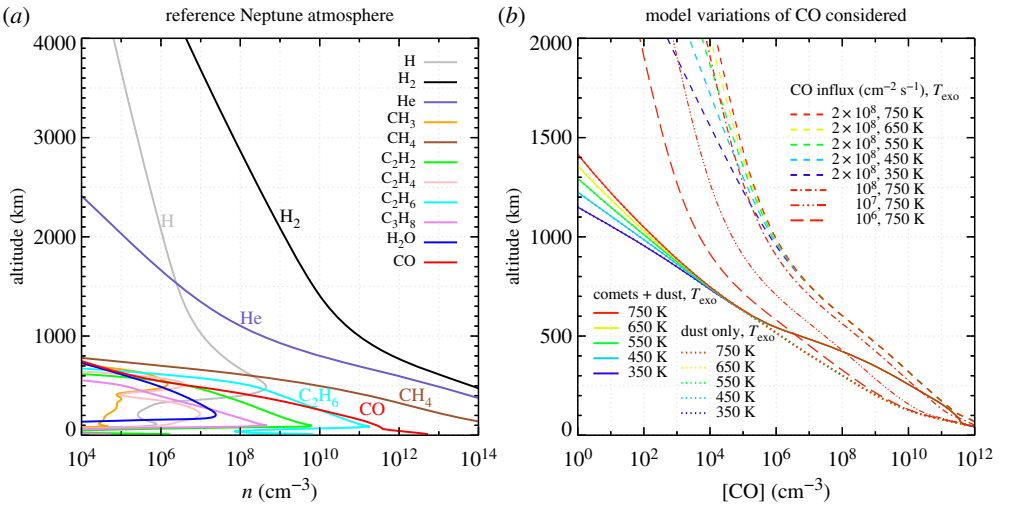

Figure 2. (*a*) Reference Neptune atmosphere at 45° S planetocentric latitude with $T_{exo} = 750$ K and CO based on cometary and dust sources (see [24]), plotted in altitude to highlight the upper atmosphere. (*b*) Variations in CO considered in this work due to T_{exo} (line colours) and CO source (line types). CO from the 'dust only' and 'comet+dust' model types are identical above 600 km altitude (i.e. the dotted and solid curves overlap there). Similarly, topside CO influxes of $< 10^6$ cm^{-2} s^{-1} (not shown) are indistinguishable from the 'dust only' model below approximately 1000 km. Note that the axes are scaled differently in each panel. (Online version in colour.)

in order to compare directly with observational constraints. Finally, in 3c, we discuss the choice of CO as the representative 'external material' within the model and speculate on the possibility and source of such large influxes.

(a) Variability in H_3^+ density

The reference Neptune ionosphere model, based on figure 2*a*, is shown in figure 3*a*. It represents local noon densities at 45° S planetocentric latitude. This latitude was chosen as a reasonable compromise between the geometry of Voyager observations and recent observational constraints [10]. The Voyager 2 RSS egress was at approximately 45° S planetographic latitude (grey shading in figure 1), and the UVS exit was at 49° S (filled circle in figure 1). Recent ground-based H_3^+ observations searched for emission integrated over Neptune's dayside between 17 and 20 August 2017. Neptune's sub-solar latitude over this time period was 25° S, but the diurnally averaged solar irradiance is quite similar at 45° S. This has been demonstrated for other giant planets (e.g. [31]), as modelled H_3^+ column densities are comparable over a wide range of latitudes in the summer hemisphere.

Figure 3*b* illustrates the effect of the neutral background variations from figure 2*b* on modelled H_3^+ densities. The solid lines represent changes due to variations in atmospheric temperature, coloured according to T_{exo}. Cooler atmospheres exhibit a decreased altitudinal extent of H_3^+, consistent with the relative atmospheric collapse, but peak H_3^+ number densities are actually marginally increased due to the reduced attenuation of solar photons at higher altitudes. CO in Neptune's atmosphere for these profiles is assumed to come from interplanetary dust (IDPs) and a cometary impact 200 years ago [24]. Dotted lines, which overlap with solid lines, investigate the possibility that Neptune's CO is instead solely due to IDPs. As shown in figure 2*b*, the 'comet+dust' and 'dust only' CO scenarios differ only below approximately 600 km altitude, and therefore it is unsurprising that their effect on H_3^+ densities, which are significant only above approximately 700 km altitude, is indistinguishable. Dashed lines then examine a scenario in which an influx of 2×10^8 CO molecules cm^{-2} s^{-1} is introduced at the top of the atmosphere.

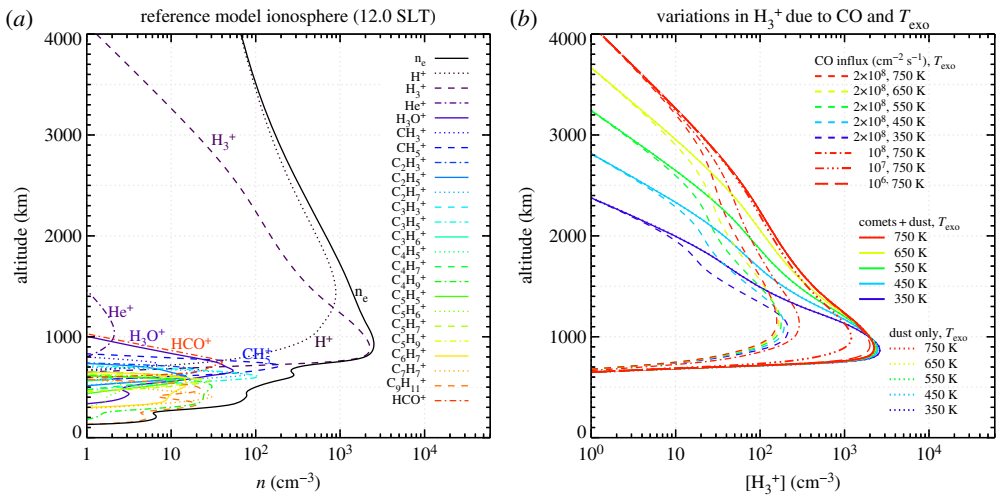

Figure 3. (*a*) Reference Neptune ionospheric model at noon solar local time (SLT). Ion species are indicated in the legend. (*b*) Variations in modelled H_3^+ at 12 SLT resulting from different T_{exo} values (line colours) and CO sources (line types). Note that, as CO from the 'dust only' and 'comet+dust' model types are identical above 600 km altitude (figure 2*b*), H_3^+ values are also identical over that region, and thus solid and dotted lines overlap completely in this panel. (Online version in colour.)

Modelled H_3^+ densities are significantly lower than either of the two previous scenarios, as H_3^+ is rapidly converted to HCO^+, though the qualitative behaviour with T_{exo} variations is similar. Finally, the remaining line types indicated in the legend examine slightly reduced topside CO influxes for the $T_{exo} = 750$ K case. From the perspective of H_3^+ density, any CO influx $< 10^6\ \mathrm{cm^{-2}\,s^{-1}}$ is effectively indistinguishable from the alternative scenarios currently used to explain stratospheric observational constraints.

(b) Comparison to observational constraints

The most recent observational constraints on H_3^+ at Neptune come from ground-based spectroscopic observations near 4 μm [10]. In that campaign, Melin *et al.* [10] aligned the spectral slit along the planetographic equator and integrated for 15.4 h over 4 nights. The 1.5 arcsec wide slit covered nearly the entire southern hemisphere of the planet, and stretched up to approximately 15° N latitude. In order to search for a faint H_3^+ emission, the data were summed spatially: i.e. integrated across Neptune's entire dayside over this region. The upper limit on spectral intensity above the continuum at the location of bright H_3^+ spectral lines was found to be $12^{+15}_{-10}\ \mathrm{nW\,m^{-2}\,sr^{-1}\,\mu m^{-1}}$. Combined with an estimated temperature of 550 K near the H_3^+ peak, this led to an upper limit on H_3^+ column density of $1.0^{+1.2}_{-0.16} \times 10^{13}\ \mathrm{m^{-2}}$, a 30% improvement over previous constraints [15,16].

In order to best compare with observations, which are column integrated, we must derive similar modelled parameters. However, as H_3^+ emission is tightly coupled to the vertical temperature and gradients present in the atmosphere, and as imperfect knowledge of those gradients can induce ambiguity in the derived column-integrated densities and temperatures [31], it is best to compare with the more fundamental upper limit on H_3^+ emission rather than the derived column density. Therefore, figure 4 presents model results for both H_3^+ column densities (4*a*) and total emission (4*b*). These are mean daytime values, meaning they are the average from 6 to 18 solar local time (SLT), consistent with the observations. Column densities follow directly from figure 3*b*. Total H_3^+ emission is calculated by combining the line list of Neale *et al.* [56] with the partition function and total emission formulation of Miller *et al.* [57]. This treatment depends

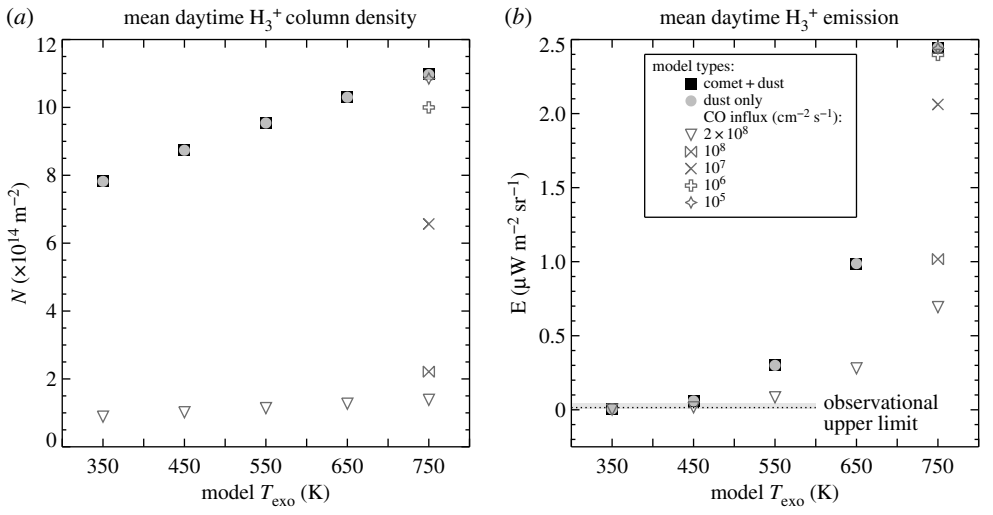

Figure 4. (*a*) Mean daytime (= 6–18 SLT here) H_3^+ column density for each model simulation. (*b*) Mean daytime (6–18 SLT) H_3^+ emission for each model simulation. Symbols and colours in the legend represent modelled variations in CO (shown in figure 2), while T_{exo} variations are indicated along the abscissa. The grey shaded region, split by a dotted line, indicates the upper limit, including error bars, on H_3^+ emission from ground-based observations [10].

on the vertical structure of both H_3^+ density and temperature. H_3^+ has been found to be in quasi-LTE with the surrounding neutral atmosphere at the other giant planets, at least at altitudes within ~5 scale heights of the density peak (e.g. [58,59]). Therefore, we take the H_3^+ temperature to be the neutral temperature (figure 1) for these calculations.

Based on figure 4*a*, H_3^+ column density is most strongly affected by enhanced CO influxes. An atmosphere with T_{exo} of 350 K has a column density that is 30% lower than one with T_{exo} of 750 K, whereas the impact of a CO influx of 2×10^8 cm^{-2} s^{-1} leads to a reduction by more than a factor of 10. This relative importance of CO influx is minimized for cooler atmospheres, however. In figure 4*b*, showing total H_3^+ emission, the situation is reversed and temperature becomes the more important parameter. If Neptune's atmosphere is still as warm as it was during the Voyager 2 flyby ($T_{exo} = 750$ K), then H_3^+ emission could vary by more than a factor of 3, depending on the thermospheric CO concentration. However, H_3^+ emission drops off precipitously with cooler and cooler atmospheres, to the point that CO influx has no noticeable impact on the already weak emission when T_{exo} is ≤ 450 K.

The grey shaded region and dotted line in figure 4*b* represent the observational limits from Melin *et al.* [10], recast in terms of total H_3^+ emission. The model atmospheres with T_{exo} of 350 K and 450 K are consistent with the observations, regardless of the thermospheric CO content. When we consider that there remain a number of model input paramaters that we have not varied here, it is possible that the $T_{exo} = 550$ K atmosphere is also consistent with these constraints, provided there is a topside CO influx of 2×10^8 cm^{-2} s^{-1}. It is clear, however, that no reasonable combination of model parameters is consistent with the present non-detection of H_3^+ at Neptune when the atmosphere is warm. Modelled H_3^+ total emission for both the T_{exo} 650 K and 750 K cases far exceeds the observational upper limit of $15^{+42}_{-3.3}$ nW m^{-2} sr^{-1}, regardless of CO input.

(c) Discussion of external influx

Based on figure 4*b*, there is at least one scenario where the maximum-allowed CO influx of 2×10^8 cm^{-2} s^{-1} could help explain the lack of H_3^+ detection: when T_{exo} is also 550 K. None of the

other reduced CO influxes considered can sufficiently remove H_3^+ in the thermosphere. If this large CO influx is real, where does it come from?

Triton, as an active moon, is one possible source, though current estimates for atmospheric escape from Triton are much smaller than the CO fluxes considered here. For example, based largely on Voyager data, a range of studies find N, N_2, N^+ and hydrogen escape rates roughly of order $10^{25}\,s^{-1}$ [60–65]. Deposited globally at Neptune, this would translate to influxes of approximately $10^5\,cm^{-2}\,s^{-1}$. However, the CO/N_2 mixing ratio at Triton is approximately 6×10^{-4}, meaning CO escape rates and resulting influxes are likely even lower. Of course, these external influxes may be concentrated locally at Neptune, such as at low latitudes, like Encealadus' plumes at Saturn [66], but likely not as drastically as would be required, and in any case such local concentration would only mean H_3^+ at other latitudes remained undiminished. That said, CO in Triton's atmosphere appears to be controlled by seasonal transport and/or atmospheric escape [67], and it may not be in steady-state [68]. Therefore, Triton remains an unlikely but intriguing possibility as the source of CO considered here.

Neptune's dusty rings present another appealing possible source of ionospheric contaminant. During the Cassini spacecraft's end-of-mission proximal orbits, mass fluxes into Saturn's atmosphere of up to $20 \times 10^4\,kg\,s^{-1}$ were derived from *in situ* measurements of infalling ring material [52,53,69,70], leading to significant modification of its equatorial ionosphere [11,71,72]. Cassini Ion and Neutral Mass Spectrometer spectra in Saturn's upper atmosphere were unexpectedly rich [52], showing stable signal out to 100 mass per charge (u), with a strong 28u peak containing significant CO contribution [73]. Neptune's rings are of course less massive than Saturn's, but the implicated source at Saturn was the tenuous D68 ringlet [52]. The bulk of the ring mass flux measured by Cassini was concentrated at Saturn's equator, yet there were still substantial charged particle 'ring rain' effects on mid-latitude H_3^+ concentrations [8,53]. Therefore, Neptune's rings as a source of ionospheric modification remain as a possibility.

4. Conclusion

H_3^+ has regularly been monitored at all of the giant planets except Neptune. Current observational upper limits on H_3^+ column density are at least a factor of 5 lower than straightforward ionospheric models predict; however, these upper limits are also based on Voyager 2 temperature measurements from approximately 30 years ago. In order to address these model-data discrepancies, we performed model explorations of two primary factors that could affect H_3^+ emission: variations in upper atmospheric temperature, and variations in thermospheric CO concentration due to enhanced topside influxes.

As H_3^+ emission is driven exponentially by temperature, the simplest way to generate an ionosphere consistent with the H_3^+ upper limits is to reduce the upper atmospheric temperature. We find that if the topside temperature, T_{exo}, is $\leq 450\,K$, then modelled H_3^+ emission is within current constraints. For warmer atmospheres, up to T_{exo} of 550 K, H_3^+ density must be reduced significantly to avoid exceeding the H_3^+ emission upper limit. A topside CO influx of $2 \times 10^8\,cm^{-2}\,s^{-1}$ could fill this role by converting H_3^+ to HCO^+. (Larger topside CO influxes would lead to stratospheric abundances in excess of current observations [24].) In this scenario, the HCO^+ column density is modelled to be $4.3 \times 10^{14}\,m^{-2}$. Therefore, if H_3^+ continues to evade detection, and if there is indeed a significant CO influx present, then it might be possible to observe HCO^+ instead. Such a measurement could place a soft constraint on the topside CO influx, and thus be used to infer thermospheric temperatures when combined with H_3^+ upper limits.

The potential for Neptune's atmosphere to be significantly cooler than what Voyager 2 found is intriguing, and would also have important implications for any future spacecraft considering aerobraking as a means of orbital insertion. Furthermore, with the James Webb Space Telescope and other advanced facilities coming online in the next decade, the possibility of using H_3^+ as a probe of Neptune's upper atmosphere, as at the other giant planets, is significantly increased. The explanation behind the high observed exospheric temperatures at the giant planets is a

longstanding problem, and measurements of H_3^+ at Neptune could help by expanding the available comparative planetary studies.

Data accessibility. Only model 'data' were used here and are available from L.M. upon request.

Authors' contributions. L.M. conceived of and designed the study, performed the ionospheric simulations and drafted the manuscript. J.I.M. contributed to the design of the study, and performed neutral model simulations. H.M., T.S.S. and J.O'D. performed the Neptune H_3^+ observations (H.M. as lead), and advised on H_3^+ emission calculations. All authors reviewed, edited and approved the manuscript.

Competing interests. We declare we have no competing interests.

Funding. L.M. and J.I.M. were supported by the National Aeronautics and Space Administration (NASA) under grant no. 80NSSC19K0546 issued through the Solar System Workings Program.

Acknowledgements. We are grateful to the TIMED/SEE PI, Tom Woods, and his team for providing us with the solar flux dataset and associated routines for extrapolation to planets.

References

1. Miller S, Tennyson J, Geballe TR, Stallard T. 2020 Thirty years of H_3^+ astronomy. *Rev. Mod. Phys.* **92**, 035003. (doi:10.1103/RevModPhys.92.035003)
2. Oka T. 2019 H_3^+, the ideal probe for *in situ* measurement of the Galactic cosmic rays. *Phil. Trans. R. Soc. A* **377**, 20180402. (doi:10.1098/rsta.2018.0402)
3. Drossart P *et al.* 1989 Detection of H_3^+ on Jupiter. *Nature* **340**, 539–541. (doi:10.1038/340539a0)
4. Johnson R, Melin H, Stallard T, Tao C, Nichols J, Chowdhury M. 2018 Mapping H_3^+ temperatures in Jupiter's Northern auroral ionosphere using VLT-CRIRES. *J. Geophys. Res. A: Space Phys.* **123**, 1–19. (doi:10.1002/jgra.53785)
5. Uno T, Kasaba Y, Tao C, Sakanoi T, Kagitani M, Fujisawa S, Kita H, Badman SV. 2014 Vertical emissivity profiles of Jupiter's northern H_3^+ and H2 infrared auroras observed by Subaru/IRCS. *J. Geophys. Res.: Space Phys.* **119**, 10 219–10 241. (doi:10.1002/2014ja020454)
6. Dinelli BM, Adriani A, Mura A, Altieri F, Migliorini A, Moriconi ML. 2019 JUNO/JIRAM's view of Jupiter's H_3^+ emissions. *Phil. Trans. R. Soc. A* **377**, 20180406. (doi:10.1098/rsta.2018.0406)
7. Stallard TS *et al.* 2019 Local-time averaged maps of H_3^+ emission, temperature and ion winds. *Phil. Trans. R. Soc. A* **377**, 20180405. (doi:10.1098/rsta.2018.0405)
8. O'Donoghue J, Moore L, Connerney J, Melin H, Stallard TS, Miller S, Baines KH. 2018 Observations of the chemical and thermal response of 'ring rain' on Saturn's ionosphere. *Icarus* **322**, 251–260. (doi:10.1016/j.icarus.2018.10.027)
9. Melin H *et al.* 2019 The H_3^+ ionosphere of Uranus: decades-long cooling and local-time morphology. *Phil. Trans. R. Soc. A* **377**, 20180408. (doi:10.1098/rsta.2018.0408)
10. Melin H, Fletcher LN, Stallard TS, Johnson RE, O'Donoghue J, Moore L, Donnelly PT. 2018 The quest for H_3^+ at Neptune: deep burn observations with NASA IRTF iSHELL. *Mon. Not. R. Astron. Soc.* **474**, 3714–3719. (doi:10.1093/mnras/stx3029)
11. Moore L *et al.* 2018 Models of Saturn's equatorial ionosphere based on *in situ* data from Cassini's grand finale. *Geophys. Res. Lett.* **45**, 1–10. (doi:10.1002/grl.56368)
12. Broadfoot AL *et al.* 1989 Ultraviolet spectrometer observations of Neptune and Triton. *Science* **246**, 1459–66. (doi:10.1126/science.246.4936.1459)
13. Yelle RV, Herbert F, Sandel BR, Vervack Jr RJ, Wentzel TM. 1993 The distribution of hydrocarbons in Neptune's upper atmosphere. *Icarus* **104**, 38–59. (doi:10.1006/icar.1993.1081)
14. Bishop J, Atreya SK, Romani PN, Sandel BR, Herbert F. 1992 Voyager 2 ultraviolet spectrometer solar occultations at Neptune: constraints on the abundance of methane in the stratosphere. *J. Geophys. Res.* **97**, 11681. (doi:10.1029/92JE00959)
15. Feuchtgruber H, Encrenaz T. 2003 The infrared spectrum of Neptune at 3.5–4.1 microns: search for H3+ and evidence for recent meteorological variations. *Astron. Astrophys.* **403**, 7–10. (doi:10.1051/0004-6361:20030414)
16. Melin H, Stallard T, Miller S, Lystrup MB, Trafton LM, Booth TC, Rivers C. 2011 New limits on H3+ abundance on Neptune using Keck NIRSPEC. *Mon. Not. R. Astron. Soc.* **410**, 641–644. (doi:10.1111/j.1365-2966.2010.17468.x)
17. Oka T. 2012 Chemistry, astronomy and physics of H3+. *Phil. Trans. R. Soc. A* **370**, 4991–5000. (doi:10.1098/rsta.2012.0243)

18. Lam HA, Achilleos N, Miller S, Tennyson J, Trafton LM, Geballe TR, Ballester GE. 1997 A baseline spectroscopic study of the infrared auroras of Jupiter. *Icarus* **393**, 379–393. (doi:10.1006/icar.1997.5698)
19. Lyons JR. 1995 Metal ions in the atmosphere of Neptune. *Science* **267**, 648–651. (doi:10.1126/science.7839139)
20. Lindal G. 1992 The atmosphere of Neptune: an analysis of radio occultation data acquired with Voyager 2. *Astron. J.* **103**, 967–982. (doi:10.1086/116119)
21. Dobrijevic M, Loison JC, Hue V, Cavalié T, Hickson KM. 2020 1D photochemical model of the ionosphere and the stratosphere of Neptune. *Icarus* **335**, 113375. (doi:10.1016/j.icarus.2019.07.009)
22. Moore L, Galand M, Kliore AJ, Nagy AF, O 'Donoghue J. 2018 Saturn's Ionosphere. In *Saturn in the 21st Century* (eds KH Baines, FM Flasar, N Krupp, TS Stallard). Cambridge, UK: Cambridge University Press; p. arXiv:1701.05178.
23. Schunk RW, Nagy AF. 2009 *Ionospheres: physics, plasma physics, and chemistry*, 2nd edn. Cambridge, UK: Cambridge University Press.
24. Moses JI, Poppe AR. 2017 Dust ablation on the giant planets: consequences for stratospheric photochemistry. *Icarus* **297**, 33–58. (doi:10.1016/j.icarus.2017.06.002)
25. Moses JI. 1992 Meteoroid ablation in Neptune's atmosphere. *Icarus* **99**, 368–383. (doi:10.1016/0019-1035(92)90153-X)
26. Moses J. 1997 Dust ablation during the Shoemaker-Levy 9 impacts. *J. Geophys. Res.* **102**, 21 619–21 643. (doi:10.1029/97JE02047)
27. Allen M, Yung YL, Waters JW. 1981 Vertical transport and photochemistry in the terrestrial mesosphere and lower thermosphere (50–120 km). *J. Geophys. Res.* **86**, 3617–3627. (doi:10.1029/JA086iA05p03617)
28. Yung YL, Allen M, Pinto JP. 1984 Photochemistry of the atmosphere of Titan: comparison between model and observations. *Astrophys. J. Suppl. Ser.* **55**, 465–506. (doi:10.1086/190963)
29. Moses JI, Armstrong ES, Fletcher LN, Friedson AJ, Irwin PG, Sinclair JA, Hesman BE. 2015 Evolution of stratospheric chemistry in the Saturn storm beacon region. *Icarus* **261**, 149–168. (doi:10.1016/j.icarus.2015.08.012)
30. Poppe AR. 2016 An improved model for interplanetary dust fluxes in the outer solar system. *Icarus* **264**, 369–386. (doi:10.1016/j.icarus.2015.10.001)
31. Moore L, Melin H, O'Donoghue J, Stallard TS, Moses JI, Galand M, Miller S, Schmidt CA. 2019 Modelling H_3^+ in planetary atmospheres: effects of vertical gradients on observed quantities. *Phil. Trans. R. Soc. A* **377**, 20190067. (doi:10.1098/rsta.2019.0067)
32. Moore LE, Mendillo M, Müller-Wodarg ICF, Murr DL. 2004 Modeling of global variations and ring shadowing in Saturn's ionosphere. *Icarus* **172**, 503–520. (doi:10.1016/j.icarus.2004.07.007)
33. Rishbeth H, Garriott OK. 1969 *Introduction to ionospheric physics*, vol. 14, 1st edn. New York, NY: Academic Press.
34. Galand M, Moore L, Charnay B, Mueller-Wodarg I, Mendillo M. 2009 Solar primary and secondary ionization at Saturn. *J. Geophys. Res.* **114**, A06313. (doi:10.1029/2008JA013981)
35. Woods TN, Eparvier FG, Bailey SM, Chamberlin PC, Lean J, Rottman GJ, Solomon SC, Tobiska WK, Woodraska DL. 2005 Solar EUV experiment (SEE): mission overview and first results. *J. Geophys. Res.* **110**, A01312. (doi:10.1029/2004JA010765)
36. Waite JH, Cravens TE. 1987 Current review of the Jupiter, Saturn, and Uranus ionospheres. *Adv. Space Res.* **7**, 119–134. (doi:10.1016/0273-1177(87)90210-9)
37. Majeed T, Waite Jr JH, Bougher SW, Yelle RV, Gladstone GR, McConnell JC, Bhardwaj A. 2004 The ionospheres–thermospheres of the giant planets. *Adv. Space Res.* **33**, 197–211. (doi:10.1016/j.asr.2003.05.009)
38. Kim Y, Fox J. 1994 The chemistry of hydrocarbon ions in the Jovian ionosphere. *Icarus* **112**, 310–324. (doi:10.1006/icar.1994.1186)
39. Huestis DL. 2008 Hydrogen collisions in planetary atmospheres, ionospheres, and magnetospheres. *Planet. Space Sci.* **56**, 1733–1743. (doi:10.1016/j.pss.2008.07.012)
40. Huestis DL, Bougher SW, Fox JL, Galand M, Johnson RE, Moses JI, Pickering JC. 2008 Cross sections and reaction rates for comparative planetary aeronomy. *Space Sci. Rev.* **139**, 63–105. (doi:10.1007/s11214-008-9383-7)
41. Majeed T, McConnell J, Yelle R. 1991 Vibrationally excited H2 in the outer planets thermosphere: fluorescence in the Lyman and Werner bands. *Planet. Space Sci.* **39**, 1591–1606. (doi:10.1016/0032-0633(91)90085-O)

42. Orton GS, Fletcher LN, Moses JI, Lellouch E, Moreno R, Swinyard BM, Hofstadter MD, Greathouse TK. 2014 Thermal emission constraints on the atmospheres of Uranus and Neptune. In *Workshop on the Study of the Ice Giant Planets, LPI Contributions*, p. 2002.
43. Moses JI, Fletcher LN, Greathouse TK, Orton GS, Hue V. 2018 Seasonal stratospheric photochemistry on Uranus and Neptune. *Icarus* **307**, 124–145. (doi:10.1016/j.icarus.2018.02.004)
44. Feuchtgruber H *et al.* 2013 The D/H ratio in the atmospheres of Uranus and Neptune from Herschel-PACS observations. *Astron. Astrophys.* **126**, 1–9. (doi:10.1051/0004-6361/201220857)
45. Koskinen TT, Sandel BR, Yelle RV, Strobel DF, Müller-Wodarg ICF, Erwin JT. 2015 Saturn's variable thermosphere from Cassini/UVIS occultations. *Icarus* **260**, 174–189. (doi:10.1016/j.icarus.2015.07.008)
46. Brown Z, Koskinen T, Müller-Wodarg I, West R, Jouchoux A, Esposito L. 2020 A pole-to-pole pressure–temperature map of Saturn's thermosphere from Cassini Grand Finale data. *Nat. Astron.* **2020**, 1–8. (doi:10.1038/s41550-020-1060-0)
47. Miller S, Aylward A, Millward G. 2005 Giant planet ionospheres and thermospheres: the importance of ion-neutral coupling. *Space Sci. Rev.* **116**, 319–343. (doi:10.1007/s11214-005-1960-4)
48. Matcheva KI, Strobel DF. 2001 Interaction of gravity waves with ionospheric plasma: implications for Jupiter's ionosphere. *Icarus* **152**, 347–365. (doi:10.1006/icar.2001.6631)
49. Matcheva KI, Barrow DJ. 2012 Small-scale variability in Saturn's lower ionosphere. *Icarus* **221**, 525–543. (doi:10.1016/j.icarus.2012.08.022)
50. Yelle RV, Miller S. 2004 Jupiter's Thermosphere and Ionosphere. In *Jupiter: The Planet, Satellites and Magnetosphere* (eds F Bagenal, TE Dowling, WB McKinnon), pp. 185–218. Cambridge, UK: Cambridge University Press.
51. Miller S, Stallard T, Tennyson J, Melin H. 2013 Cooling by H_3^+ emission. *J. Phys. Chem. A* **117**, 9770–9777. (doi:10.1021/jp312468b)
52. Waite JHJ *et al.* 2018 Chemical interactions between Saturn's atmosphere and rings. *Science* **362**, 1–12.
53. Hsu Hw *et al.* 2018 Cosmic dust analyzer onboard cassini collects material from Saturn's main rings. *Science* **362**, eaat3185. (doi:10.1126/science.aat3185)
54. Barrow DJ, Matcheva KI. 2013 Modeling the effect of atmospheric gravity waves on Saturn's ionosphere. *Icarus* **224**, 32–42. (doi:10.1016/j.icarus.2013.01.027)
55. Lellouch E, Moreno R, Paubert G. 2005 A dual origin for Neptune's carbon monoxide? *Astron. Astrophys.* **430**, L37–L40. (doi:10.1051/0004-6361:200400127)
56. Neale L, Miller S, Tennyson J. 1996 Spectroscopic properties of the H3+ molecule: a new calculated line list. *Astrophys. J.* **464**, 516–520. (doi:10.1086/177341)
57. Miller S, Stallard T, Melin H, Tennyson J. 2010 H3+ cooling in planetary atmospheres. *Faraday Discuss.* **147**, 283. (doi:10.1039/c004152c)
58. Moore L, Galand M, Müller-Wodarg I, Yelle R, Mendillo M. 2008 Plasma temperatures in Saturn's ionosphere. *J. Geophys. Res.* **113**, A10306. (doi:10.1029/2008JA013373)
59. Tao C, Badman SV, Fujimoto M. 2011 UV and IR auroral emission model for the outer planets: Jupiter and Saturn comparison. *Icarus* **213**, 581–592. (doi:10.1016/j.icarus.2011.04.001)
60. Yung YL, Lyons JR. 1990 Triton: topside ionosphere and nitrogen escape. *Geophys. Res. Lett.* **17**, 1717–1720. (doi:10.1029/GL017i010p01717)
61. Strobel DF, Summers ME. 1990 The photochemistry of methane in the atmosphere of Triton. *Geophys. Res. Lett.* **17**, 1729–1732. (doi:10.1029/GL017i010p01729)
62. Sandel BR, Herbert F, Dessler AJ, Hill TW. 1990 Aurora and airglow on the night side of Neptune. *Geophys. Res. Lett.* **17**, 1693–1696. (doi:10.1029/GL017i010p01693)
63. Summers ME, Strobel DF. 1991 Triton's atmosphere: a source of N and H for Neptune's magnetosphere. *Geophys. Res. Lett.* **18**, 2309–2312. (doi:10.1029/91GL01334)
64. Krasnopolsky VA, Sandel BR, Herbert F, Vervack Jr RJ. 1993 Temperature, N2, and N density profiles of Triton's atmosphere: observations and model. *Geophys. Res. Lett.* **98**, 3065–3078. (doi:10.1029/92JE02680)
65. Lammer H. 1995 Mass loss of N2 molecules from Triton by magnetospheric plasma interaction. *Planet. Space Sci.* **43**, 845–850. (doi:10.1016/0032-0633(94)00214-C)
66. Fleshman BL, Delamere PA, Bagenal F, Cassidy T. 2012 The roles of charge exchange and dissociation in spreading Saturn's neutral clouds. *J. Geophys. Res.* **117**, E05007. (doi:10.1029/2011JE003996)

67. Lellouch E, Bergh CD, Sicardy B, Ferron S, Käufl HU. 2010 Detection of CO in Triton's atmosphere and the nature of surface-atmosphere interactions. *Astron. Astrophys.* **512**, 2–7. (doi:10.1051/0004-6361/201014339)
68. Elliot JL, Strobel DF, Zhu X, Stansberry JA, Wasserman LH, Franz OG. 2000 The thermal structure of Triton's middle atmosphere. *Icarus* **143**, 425–428. (doi:10.1006/icar.1999.6312)
69. Perry ME, Jr JHW, Mitchell DG, Miller KE, Cravens TE. 2018 Material flux from the rings of Saturn into its atmosphere. *Geophys. Res. Lett.* **45**, 1–8. (doi:10.1029/2018GL078575)
70. Mitchell DG *et al.* 2018 D-ring dust falling into Saturn's equatorial upper atmosphere. *Science* **362**, 50. (doi:10.1126/science.aat2236)
71. Cravens TE, Moore L, Waite Jr JH, Perryman R, Perry M, Wahlund JE, Persoon A, Kurth WS. 2018 The ion composition of Saturn's equatorial ionosphere as observed by Cassini. *Geophys. Res. Lett.* **46**, 6315–6321. (doi:10.1029/2018GL077868)
72. Morooka MW *et al.* 2019 Saturn's dusty ionosphere. *J. Geophys. Res. A: Space Phys.* **124**, 1679–1697. (doi:10.1029/2018JA026154)
73. Miller KE *et al.* 2020 Cassini INMS constraints on the composition and latitudinal fractionation of Saturn ring rain material. *Icarus* **339**, 113595. (doi:10.1016/j.icarus.2019.113595)